Luteolin induces apoptosis by impairing mitochondrial function and targeting the intrinsic apoptosis pathway in gastric cancer cells

JUN MA[1,2], ZHAOHAI PAN[2], HONGCHAO DU[3], XIAOJIE CHEN[2], XUEJIE ZHU[2], WENJIN HAO[4], QIUSHENG ZHENG[2,5] and XUEXI TANG[1]

[1]College of Marine Life Sciences, Ocean University of China, Qingdao, Shandong 266003; [2]Yantai Key Laboratory of Pharmacology of Traditional Chinese Medicine in Tumor Metabolism, School of Integrated Traditional Chinese and Western Medicine, Binzhou Medical University, Yantai, Shandong 264003; [3]Department of General Surgery, Binzhou Medical University Affiliated Yantai Yeda Hospital, Yantai, Shandong 265599; [4]School of Life Sciences, Nantong University, Nantong, Jiangsu 226019; [5]Key Laboratory of Xinjiang Endemic Phytomedicine Resources, Pharmacy School, Shihezi University, Shihezi, Xinjiang 832099, P.R. China

Received February 18, 2022; Accepted March 29, 2023

DOI: 10.3892/ol.2023.13913

Abstract. Gastric cancer is one of the most lethal cancers worldwide. Research has focused on exploring natural medicines to improve the systematic chemotherapy for gastric cancer. Luteolin, a natural flavonoid, possesses anticancer activities. Nevertheless, the mechanism of the anticancer effects of luteolin is still not clear. The present study aimed to verify the inhibitory effect of luteolin on gastric cancer HGC-27, MFC and MKN-45 cells and to explore the underlying mechanism. A Cell Counting Kit-8 cell viability assay, flow cytometry, western blot, an ATP content assay and an enzyme activity testing assay were used. Luteolin inhibited the proliferation of gastric cancer HGC-27, MFC and MKN-45 cells. Further, it impaired mitochondrial integrity and function by destroying the mitochondrial membrane potential, downregulating the activities of mitochondrial electron transport chain complexes (mainly complexes I, III and V), and unbalancing the expression of B cell lymphoma-2 family member proteins, eventually leading to apoptosis of gastric cancer HGC-27, MFC and MKN-45 cells. The intrinsic apoptosis pathway was involved in luteolin's anti-gastric cancer effects. Furthermore, mitochondria were the main target in luteolin-induced gastric cancer apoptosis. The present study may provide a theoretical basis for the research on the effect of luteolin on the mitochondrial metabolism in cancer cells, and pave the way for its practical application in the future.

Correspondence to: Professor Xuexi Tang, College of Marine Life Sciences, Ocean University of China, 5 Yushan Road, Shinan, Qingdao, Shandong 266003, P.R. China
E-mail: tangxx@ouc.edu.cn

Abbreviations: Bax, Bcl-2-associated X; Bcl-2, B cell lymphoma-2; HGC-27, human gastric cancer HGC-27 cell line; METC, mitochondrial electron transport chain; MFC, mouse forestomach carcinoma cell line; MMP, mitochondrial membrane potential; ROS, reactive oxygen species

Key words: luteolin, apoptosis, mitochondria, mitochondrial electron transport chain, B cell lymphoma-2 family, gastric cancer cell

Introduction

Gastric cancer is the fifth most common cancer around the world; although its overall incidence has been declining in recent years, it still ranks as the third cause of cancer-related death (1). Clinical treatment is radical and involves a combination of surgery and chemical therapy (2). Effective constituents from traditional herbal medicines, such as paclitaxel, are often preferred for the development of chemical drugs (3). The introduction of novel bioactive components of natural origin may be considered as a new and reliable chemotherapeutic strategy for different types of human cancer based on their selective molecular targets (4). Currently, much attention has been focused on search for natural medical ingredients as novel chemotherapeutic agents for cancer.

Luteolin, 3',4',5,7-tetrahydroxyflavone, is a traditional herbal medical ingredient, belonging to the flavonoid family (4). Luteolin is the main constituent of *Ajuga decumbens thunb*, which is broadly used for cough suppression, expectoration, and inflammation control. At present, an increasing number of studies are being carried out focusing on new pharmacological activities of luteolin, including neuroprotection, antiinflammation, antioxidation, and antibacterial action (4). It is reported that luteolin exerts inhibitory effects on cell proliferation, metastasis, invasion, and angiogenesis through multiple pathways (5). Despite some progress, the mechanism of luteolin's anticancer effects is still largely unknown (6). Therefore, this work focused on the inhibitory effects of luteolin on gastric cancer cells' proliferation and explored the underlying mechanism.

Regarding carcinogenesis, mitochondria are distinctly important organelles that provide bioenergy for cancer cells' proliferation and metastasis and regulate the apoptosis pathway under certain stimuli (7,8). Apoptosis occurs through two classic pathways: intrinsic and extrinsic (6), both of which are closely related to mitochondria. Any alteration or interruption in the mitochondrial membrane may activate both the intrinsic and extrinsic apoptosis pathways-the hallmark of apoptosis (6,9). Therefore, precisely targeting mitochondria is considered a promising approach in cancer therapy (10). The strategy of targeting mitochondria primarily focuses on the elevation of oxidative stress and destabilization of the mitochondrial membrane, ultimately inducing mitochondria-mediated apoptosis in cancer cells (7). On the outer mitochondrial membrane, the B cell lymphoma-2 (Bcl-2) family members, such as Bcl-2 and Bcl-2-associated X protein (Bax), are involved in regulating the outer mitochondrial membrane's function and the apoptotic signaling pathways. On the inner mitochondrial membrane, the mitochondrial electron transport chain (METC) plays the central role in the chemiosmotic theory (11). METC is composed of complex I (NADH-coenzyme Q oxidoreductase), complex II (succinate ubiquinone oxidoreductase), complex III (CoQ-cytochrome c oxidoreductase), cytochrome c, complex IV (cytochrome c oxidase), and complex V (F_0F_1-ATP synthase) (12). Complexes I and III, especially the former, are considered the main sites of reactive oxygen species (ROS) generation. METC complex V can utilize the proton potential from other METC complexes to phosphorylate adenosine diphosphate (ADP) to form adenosine triphosphate (ATP) (13). This is the crucial energy-generating pathway in living cells. An interruption of the electron transfer between METC complexes might be associated with ROS elevation. Meanwhile, it has been reported that METC is closely associated with cancer cell apoptosis. Xanthohumol, a polyphenol, effectively induces apoptosis and mitochondrial superoxide generation by inhibiting the activities of complexes I and III and by restraining the electron transfer between them, followed by cytochrome c release from mitochondria (14).

Due to the contribution of mitochondria to cancer cell survival, targeting the mitochondria is a plausible and intriguing strategy to eliminate cancer cells with relatively high specificity (15). Therefore, this work employed the human gastric cancer HGC-27 cell line and MKN-45 cell line, and mouse forestomach carcinoma MFC cell line to explore the anticancer effects of luteolin and to investigate the underlying mechanism. In addition, this study explores if luteolin could exert the inhibitory effects on gastric cancer cells from different species by demonstrating the different effects of luteolin on human gastric cancer cells and mouse gastric cancer cells. Moreover, the data from mouse gastric cancer cells will pave the way to the research on the effects of luteolin on the immune system in tumor-bearing mice in the future.

We aimed to identify the inhibitory effects of luteolin on gastric cancer cells proliferation and to reveal the vital role of mitochondria in luteolin-induced apoptosis in gastric cancer cells. This work may provide new insights into luteolin's anticancer effects by interfering with the mitochondrial function.

Materials and methods

Reagents. Luteolin (purity≥98%) was purchased from Sigma-Aldrich Company (L9283, St. Louis, MO, United States). Luteolin was dissolved in dimethyl sulfoxide (DMSO) (D8371, Solarbio, Beijing, China) and diluted with complete medium to the required concentration. The final concentration of DMSO in the working solution was less than 0.1%, which had no adverse effects on cell viability. The other detection reagents were bought from Sigma-Aldrich Company (St. Louis, MO, United States) and Solarbio Science & Technology Co., Ltd (Beijing, China).

Cell culture. Human gastric cancer HGC-27 cell line (1101HUM-PUMC000279), mouse forestomach carcinoma MFC cell line (1101MOU-PUMC000143), and MKN-45 cell line (1101HUM-PUMC000229) were purchased from National Infrastructure of Cell Line Resource (Beijing, China). Cells were cultured in RPMI 1640 medium (31800, Solarbio, Beijing, China) containing 10% fetal bovine serum (REF10091-148, Gibco; Thermo Fisher Scientific Inc., Massachusetts, United States) and incubated at 37˚C in a 5% CO_2 incubator (HF90/HF240, Heal Force, Shanghai, China). Subsequently, the cells were treated with different concentrations of luteolin for 24 h. RPMI 1640 complete medium containing 0.1% DMSO was used as a control.

CCK-8 cell viability assay. The effect of luteolin on cells viability was determined using the CCK-8 assay (16). Briefly, 100 μl of cell suspension per well was seeded in a 96-well plate at a density of 6,000 cells/well. After incubation for 24 h at 37˚C in a 5% CO_2 incubator (HF90/HF240, Heal Force, Shanghai, China), the supernatant was discarded, and the HGC-27 and MFC cells were treated with the different luteolin concentrations (10, 20, 30, 40, 50, 60, 70, and 80 μM in 200 μl/well) for 24 h, and MKN-45 cells were treated for 48 h. According to the cytotoxicity assay kit (CA1210, Solarbio, Beijing, China) protocol, 100 μl of working solution (CCK-8: complete RPMI 1640 medium=1:10) was added to each well. After incubation at 37˚C for 60 min in the dark, the absorbance at a wavelength of 450 nm was detected using a Thermo 3001 multi-function microplate reader (Infinite 200 PRO, Tecan Austria GmbH, Salzburg, Austria). IC_{50} indicated that the drug concentration resulted in a 50% reduction in cell survival. Experiments were repeated more than three times. In the following assays, gastric cancer cells were treated with 10, 40, and 70 μM of luteolin. In line with the IC_{50} value of three cell lines, 10, 40, and 70 μM of luteolin is set in the arithmetic sequence. Under the treatment with 10 μM, 40 μM, and 70 μM luteolin, it is feasible to collect enough cells to meet requirements for measurement accuracy, and to exhibit the difference among various groups.

Hoechst 33258 staining. Morphological characteristics of apoptosis in cell nuclei were detected by Hoechst 33258 staining (17). At least $2.0x10^5$ cells were seeded in each well of a 6-well plate. HGC-27 and MFC cells were treated with 10, 40, and 70 μM luteolin for 24 h, and MKN-45 cells were treated for 48 h. The supernatant was discarded, and the cells were fixed with a fixing agent (acetic acid: methyl alcohol=1:3)

for 30 min. Then, the fixing agent was discarded, and the cells were rinsed with phosphate-buffered saline (PBS) solution three times. Based on Hoechst 33258 stain solution (C0021, Solarbio, Beijing, China) protocol, the cells were incubated with 500 μl of the staining working solution (Hoechst 33258: PBS=1:100) at room temperature in the dark for 5-10 min. Inverted fluorescence microscopy (DMI3000, Leica, Wetzlar, Germany) was employed to record blue nuclei changes in the different groups.

Annexin V-FITC/PI double staining assay. Quantitative analysis of the percentage of apoptosis was performed with an Annexin-V FITC/PI apoptosis detection kit (CA1020, Solarbio, Beijing, China) and flow cytometry (18). At least $2.5x10^5$ cells/well were seeded in a 6-well plate. After incubation for 24 h at 37˚C in a 5% CO_2 incubator, HGC-27 and MFC cells were treated with 10, 40, and 70 μM luteolin for 24 h, and MKN-45 cells were treated for 48 h. In accordance with the manufacturer's instructions, the cells were collected and stained with fluorescein isothiocyanate (Annexin-V FITC) and propidium iodide (PI) in the dark. The fluorescence intensity was measured using a FACSCanto II flow cytometer (Becton Dickinson and Company, Franklin Lakes, United States), and the apoptotic rates were analyzed using the FACSDiva software (version 6.1.3; Becton Dickinson and Company, Franklin Lakes, United States). Experiments were repeated in HGC-27 cells (n=7), MFC cells (n=6), and MKN-45 cells (n=5).

Detection of ROS levels. The changes in ROS levels were determined using a ROS assay kit (CA1410, Solarbio, Beijing, China) and flow cytometry (17). After luteolin treatment for 24 h in HGC-27 cells and MFC cells, and for 48 h in MKN-45 cells, the cells were collected and washed with PBS. The cells were labeled with 10 μM DCFH-DA for 30 min at 37˚C in the dark in accordance with the protocol. An inverted fluorescence microscope (DMI3000, Leica, Wetzlar, Germany) was employed to detect morphological changes. A FACSCanto II flow cytometer (Becton Dickinson and Company, Franklin Lakes, United States) was applied to determine the fluorescence intensity of the stained cells, which was analyzed using the FACSDiva software (version 6.1.3; Becton Dickinson and Company, Franklin Lakes, United States). The fluorescence mean values derived from the flow cytometer in P2 were used for quantitative analysis. The data were normalized as fold changes in comparison to the DMSO group and presented as mean ± standard deviation. Experiments were repeated in HGC-27 cells (n=6), MFC cells (n=7), and MKN-45 cells (n=3).

Measurement of the mitochondrial membrane potential (MMP, ΔΨm). MMP changes were detected in the cells using an MMP assay kit (M8650, Solarbio, Beijing, China) and flow cytometry (19). The cells were treated with 10, 40, and 70 μM luteolin for 24 h or 48 h. Then, the treated cells were resuspended in a complete media and stained with a JC-1 fluorescence working solution. MMP changes were measured with the FACSCanto II flow cytometer (Becton Dickinson and Company, Franklin Lakes, United States), and the fluorescence intensity was analyzed using the FACSDiva software (version 6.1.3; Becton Dickinson and Company, Franklin Lakes, United States). The relative ratio of red fluorescence to green fluorescence was applied for quantitative analysis of the MMP changes. The data were normalized as fold changes in comparison to the DMSO group. Experiments were repeated in HGC-27 cells (n=12), MFC cells (n=11), and MKN-45 cells (n=4).

Measurement of cellular ATP levels. Intracellular ATP was quantified using an ATP assay kit (S0026, Beyotime Biotechnology, Shanghai, China) (20). After treatment, at least $5x10^6$ cells were collected in each group, followed by the addition of 300 ul of ATP lysis buffer. After centrifugation at 12,000 x g (Thermo Scientific™ Sorvall™ Legend™ Micro 17R centrifuge; Thermo Fisher Scientific Inc., Massachusetts, United States) at 4˚C for 5 min, the supernatant was collected to examine the ATP content and the protein level. The cell supernatant and ATP standard solution were diluted to the necessary concentration with the ATP lysis buffer. Then, 20 μl of the sample or standard solution was blended with 100 μl of a reaction working agent, which was tested in a 96-well plate. The fluorescence was assessed using the Thermo 3001 multi-function microplate reader (Infinite 200 PRO, Tecan Austria GmbH, Salzburg, Austria). Each sample was measured at least in triplicate. Experiments were repeated in HGC-27 cells (n=5), MFC cells (n=4), and MKN-45 cells (n=4). The data were presented as fold changes normalized to the DMSO group.

Enzyme and protein extraction and quantification. (i) Enzyme extraction was conducted as described below. At least $5x10^6$ cells were trypsinized for assays in each group. The collected cells were lysed with the corresponding enzymes' lysis buffer and ultrasonicated on ice (power 20%, ultrasonicate 3 s, interval 10 s, repeat 30 times). The quantification of enzymes protein was performed by using the BCA protein assay kit (PC0020, Solarbio, Beijing, China). Data were obtained with a microplate reader (Infinite 200 PRO, Tecan Austria GmbH, Salzburg, Austria) for absorbance at 562 nm. The amount of enzyme protein was calculated in accordance with the prescribed computational formula of the kit protocol (PC0020, Solarbio, Beijing, China).

(ii) Protein extraction was prescribed as follows (21). Cells were lysed with ice-cold RIPA buffer (R0010, Solarbio, Beijing, China) containing 0.1 M PMSF (P0100, Solarbio, Beijing, China) and a protease phosphatase inhibitor (100x) (P1261, Solarbio, Beijing, China) and incubated on ice for at least 30 min. Then, the cell lysate was centrifuged at 12,000 x g (Thermo Scientific™ Sorvall™ Legend™ Micro 17R centrifuge; Thermo Fisher Scientific Inc., Massachusetts, United States) for 10 min at 4˚C, and the supernatant was evaluated using the BCA protein assay kit (PC0020, Solarbio, Beijing, China). The absorbance was measured at 562 nm with the microplate reader (Infinite 200 PRO, Tecan Austria GmbH, Salzburg, Austria). The amount of protein was calculated in accordance with the prescribed computational formula of the kit protocol (PC0020, Solarbio, Beijing, China). The cell lysate was adjusted to 6 μg/μl with the lysate buffer and stored at -80˚C.

Analysis of Na^+/K^+-ATPase and Ca^{2+}/Mg^{2+}-ATPase enzyme activities. The activities of Na^+/K^+-ATPase and Ca^{2+}/Mg^{2+}-ATPase were assessed using the Na^+/K^+-ATPase enzyme activity assay kit (BC0065, Solarbio, Beijing China) and Ca^{2+}/Mg^{2+}-ATPase enzyme activity assay kit (BC0965, Solarbio, Beijing China), respectively. The Na^+/K^+-ATPase activity was evaluated by the concentration of inorganic phosphate (Pi) formed upon ATP hydrolysis in accordance with a previous report (22). At least $5x10^6$ cells in each group were collected for enzyme extraction. An enzyme extraction reagent was added to the reaction mixture, and the data on Na^+/K^+-ATPase activity were obtained using the microplate reader (Infinite 200 PRO, Tecan Austria GmbH, Salzburg, Austria) at 660 nm absorbance. Experiments were repeated in HGC-27 cells (n=9) and MFC cells (n=16). Similarly, Ca^{2+}/Mg^{2+}-ATPase activity was measured by quantifying the Pi production from the conversion of ATP into ADP at 660 nm using the molybdenum blue spectrophotometric method (23). According to the protocol, one enzyme activity unit (U) was defined as μmol of inorganic phosphate liberated per $1x10^4$ cells per hour, which was quantified as results for each group. The data were presented as fold changes normalized to the DMSO group. Experiments were repeated in HGC-27 cells (n=10) and MFC cells (n=14).

Analysis of SOD activity. To detect the activity of SOD, at least $5x10^6$ cells in each group were collected after treatment. Then, SOD was extracted using an extracting solution from the SOD activity assay kit (BC0175, Solarbio, Beijing, China) (24). SOD activity was tested according to the protocol and assessed using absorbance at 560 nm with the Thermo 3001 microplate reader (Infinite 200 PRO, Tecan Austria GmbH, Salzburg, Austria). SOD activity was calculated based on the formula from the kit protocol. Relative SOD activity was calculated by normalizing the SOD activity in each group to that in the DMSO group. Each sample was measured at least in triplicate. Experiments were repeated in HGC-27 cells (n=8), MFC cells (n=6), and MKN-45 cells (n=5).

Analysis of enzyme activities of METC complexes I, III, and V. To detect the activities of METC complexes I, III, and V, at least $5x10^6$ cells were lysed in each group to obtain METC complexes, and the activities of complexes I, III, and V were further detected by using METC complex I, III, and V activity assay kits (BC0515, BC3245 and BC1440, Solarbio, Beijing, China). METC complex I activity was measured by determining the decrease in NADH absorbance at 340 nm that leads to the reduction of ubiquinone to ubiquinol (25). Cells were collected by scraping, and mitochondria were isolated on ice using the mitochondria isolation lysis of the kit. In line with the manufacturer's instructions, 10 μl of the enzyme extraction was added to 190 μl of the reaction mixture in a 96-well plate. Each sample was assessed in at least three replicates. The absorbance values at 340 nm at 10 s and 2 min were recorded with the Thermo 3001 multifunction microplate reader (Infinite 200 PRO, Tecan Austria GmbH, Salzburg, Austria). The activity was calculated using the extinction coefficient of 6.22 mM^{-1} cm^{-1} for NADH and expressed as nmol/min/mg protein. Experiments were repeated in HGC-27 cells (n=15), MFC cells (n=16), and MKN-45 cells (n=6). METC complex III activity was measured by monitoring the reduction of cytochrome c by ubiquinol at 550 nm (25). Similarly, mitochondria were isolated on ice using the isolation lysis reagent from the kit. In line with the manufacturer's instructions, 20 μl of the enzyme extraction was added to 180 μl of different reaction mixture from the testing group and the control group in a 96-well plate. The absorbance values at 550 nm at 10 s and 2 min were recorded with the Thermo 3001 multi-function microplate reader (Infinite 200 PRO, Tecan Austria GmbH, Salzburg, Austria). The activity was calculated using the extinction coefficient of $1.91x10^4$ l mol^{-1} cm^{-1} for cytochrome c and expressed as nmol/min/mg protein. Experiments were repeated in HGC-27 cells (n=6) and MFC cells (n=5). METC complex V was determined with a mitochondrial ATP-synthase assay (25). According to the instructions, the enzyme extraction was mixed with reagents for the quantitative determination of phosphorus. The ATP-synthase activity was determined as the difference between the activities obtained in the presence and absence of oligomycin. The absorbance value at 660 nm was recorded using the Thermo 3001 multi-function microplate reader (Infinite 200 PRO, Tecan Austria GmbH, Salzburg, Austria), and the results were calculated as nmol Pi/mg protein. Experiments were repeated in HGC-27 cells (n=14), MFC cells (n=14), and MKN-45 cells (n=4). All data were presented as fold changes normalized to the DMSO group.

Western blot. After the denaturation of total protein, 60 μg cell lysate from each group were separated by SDS-PAGE (a 6% spacer gel and a 10% separating gel) and transferred to a PVDF membrane (ISEQ00010, Millipore Sigma) with 200 mA constant current (Biorad Powerpac Basic 164-5050, Bio-Rad Laboratories Inc, California, United States) on ice for 2 h (17). The membranes were then blocked with 5% milk in Tris-buffered saline with Tween 20 (TBST) solution for 2 h and washed with TBST for 5 min for three times. Then, the blocked membranes were incubated in a primary antibody solution at 4˚C overnight. The primary antibodies in this work were: β-actin mouse monoclonal antibody (cat. no. TA-09; 1:2,000; OriGene Technologies Inc., Beijing, China), Bcl-2 rabbit monoclonal antibody (cat. no. ab182858; 1:1,000; Abcam, Cambridge, UK), and Bax rabbit monoclonal antibody (cat. no. ab182733; 1:1,000; Abcam, Cambridge, UK). The membranes were rinsed with TBST for 10 min three times and probed with the secondary antibody (peroxidase-conjugated goat anti-mouse IgG (H+L) (cat. no. ZB-2305; 1:50,000; OriGene Technologies Inc., Beijing, China) and goat anti-rabbit IgG (H&L) (cat. no. ab6721; 1:20,000; Abcam, Cambridge, UK)) at room temperature for 50 min. After rinsing with the TBST solution, the membranes were detected with the ECL chemiluminescence kit (WF326284, Thermo Fisher Scientific Inc., Massachusetts, United States), and visualized with the gel imaging analysis system (BioSpectrum 510 Imaging System Motorized Platform). Scanning grey analysis was performed using the Photoshop CC 2019 software (Adobe Systems Inc., California, United States). The grayscale value of each band was normalized to its corresponding β-actin. All data were presented as fold changes normalized to the DMSO group, and used to plot histograms. Experiments were repeated in

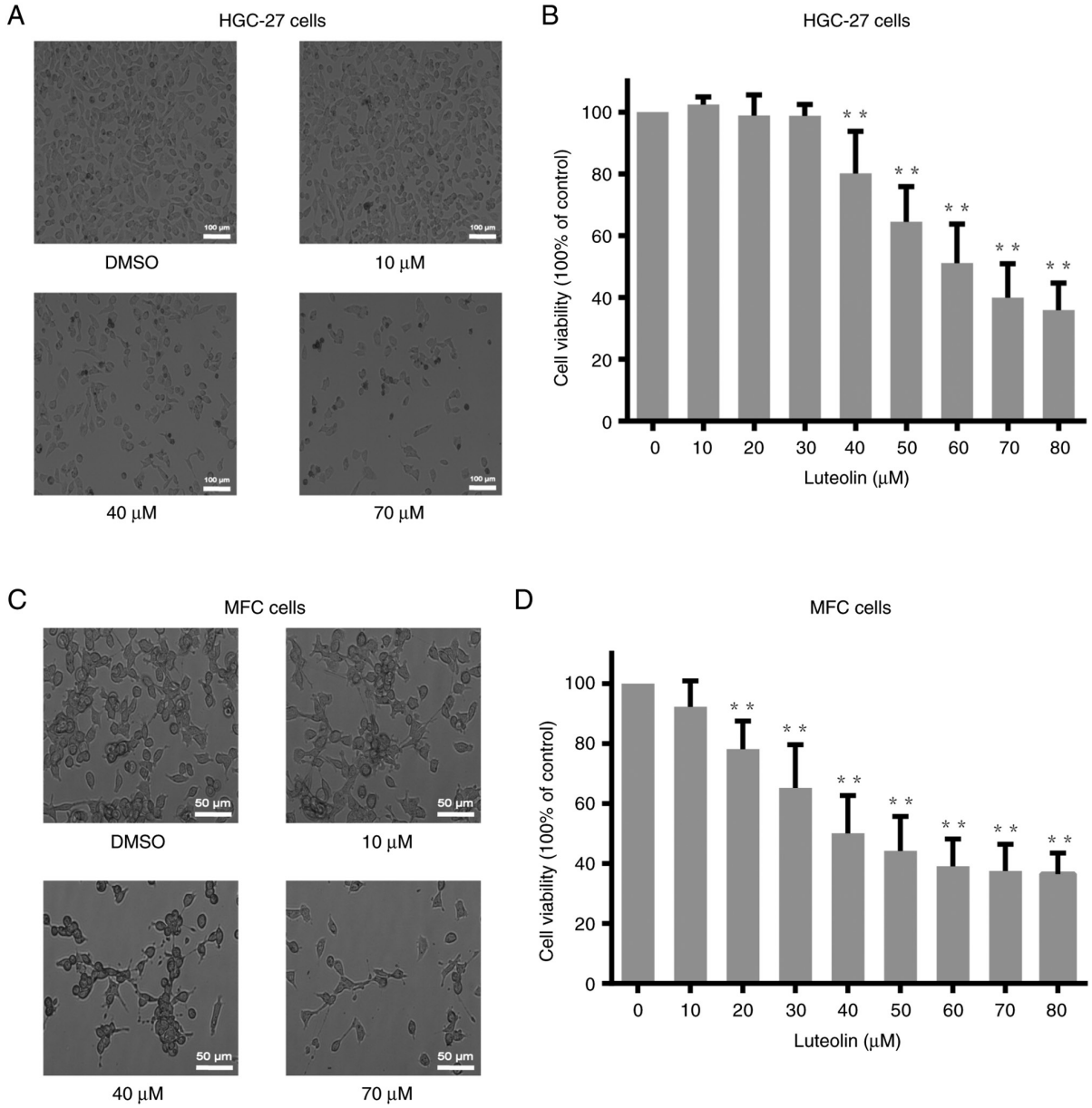

Figure 1. Viability of HGC-27 and MFC cells is affected by luteolin. HGC-27 and MFC cells were treated with different doses of luteolin for 24 h. Human gastric cancer HGC-27 cells viability was inhibited by luteolin. (A) Morphological changes of HGC-27 cells were observed under a light microscope (magnification, x100). (B) HGC-27 cell viability was detected by the Cell Counting Kit-8 assay. Mouse forestomach carcinoma MFC cells viability was inhibited by luteolin. (C) Morphological changes of MFC cells were observed under a light microscope (magnification, x200). (D) MFC cell viability was detected using the Cell Counting Kit-8 assay. The decrease in the viability rate was analyzed using the GraphPad Prism 6.0 software. Experiments were repeated at least three times. **P<0.01 vs. DMSO group. HGC-27, human gastric cancer HGC-27 cell line; MFC, mouse forestomach carcinoma cell line.

HGC-27 cells (n=6), MFC cells (n=5), and MKN-45 cells (n=5).

Statistical analysis. The experiments were carried out at least three times. Data of enzymes activities were analyzed in accordance with the prescribed calculation formula on the kit protocol. The data were normalized as fold changes to DMSO group and presented as means ± standard deviation. The analyses were performed using the SPSS 21.0 software package (version 21.0, SPSS Inc, Chicago, United States) and drew by the GraphPad Prism 6.0 software (version 6.0, GraphPad Software Inc., San Diego, United States). Statistical difference was calculated by ANOVA followed by Tukey's post hoc test. P-values less than 0.05 were considered statistically significant.

Results

Luteolin decreased gastric cancer cells viability. After treatments with different doses of luteolin (0, 10, 20, 30, 40, 50, 60, 70, and 80 μM) for 24 h or 48 h, the viability of HGC-27, MFC, and MKN-45 cells were analyzed using the CCK-8 assay. The viability of HGC-27 and MFC cells decreased in a dose-dependent manner (Fig. 1B and D), and the viability of MKN-45 cells also reduced in a dose-dependent manner (Fig. S1B). According to the cell viability analysis, the cell viability curve is created. Based on the curve, the IC_{50} value of luteolin for HGC-27 and MFC cells was approximately 60 and 40 μM, respectively. And the IC_{50} for MKN-45 at 48 h was about 50 μM. The morphological changes were

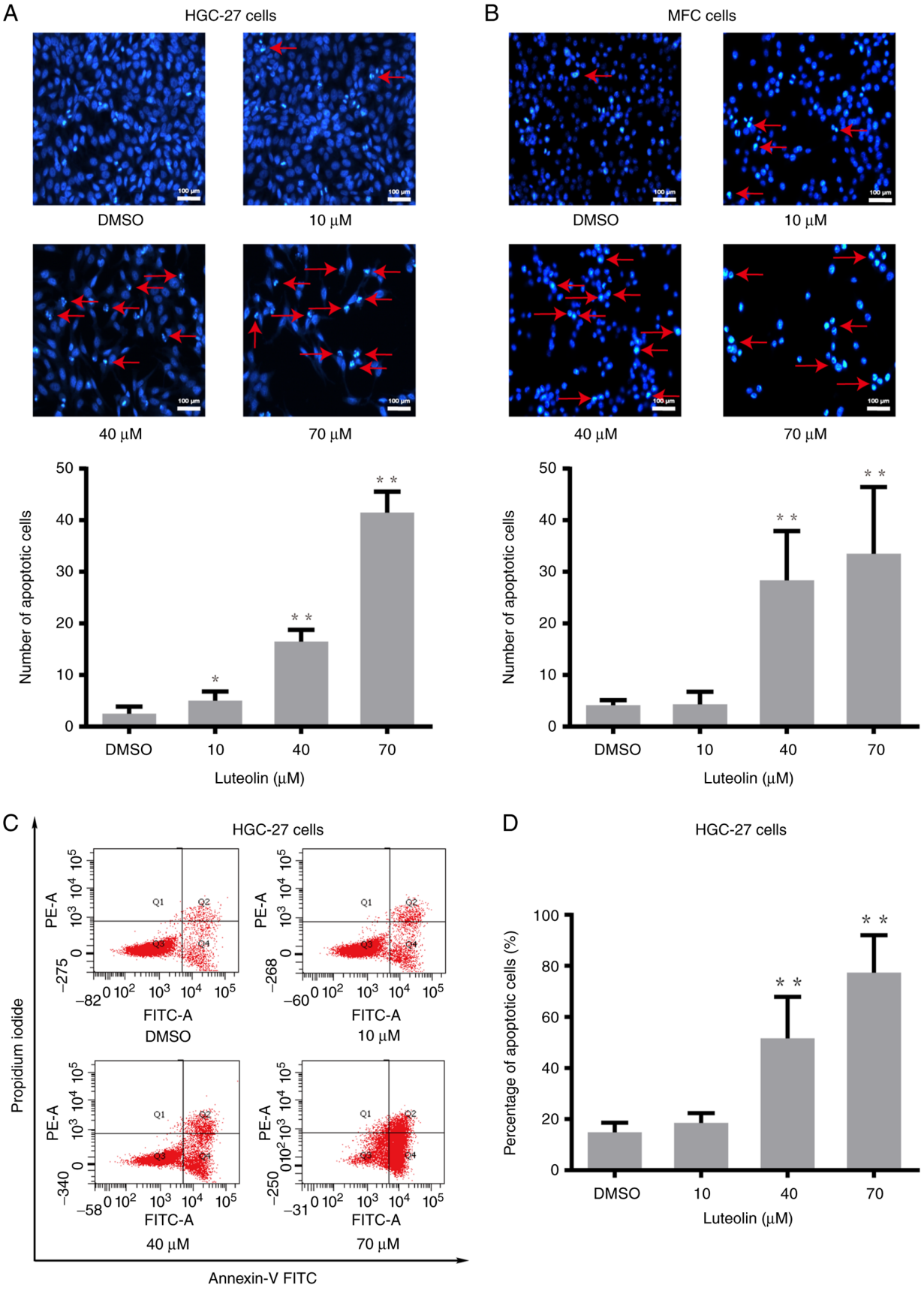

Figure 2. Continued.

observed under a light microscope, illustrating a notably reduced cell number (Figs. 1A, C, and S1A). Moreover, there are several dark speckles with lower refractive index in 40 and 70 μM, which are different with the cells in DMSO

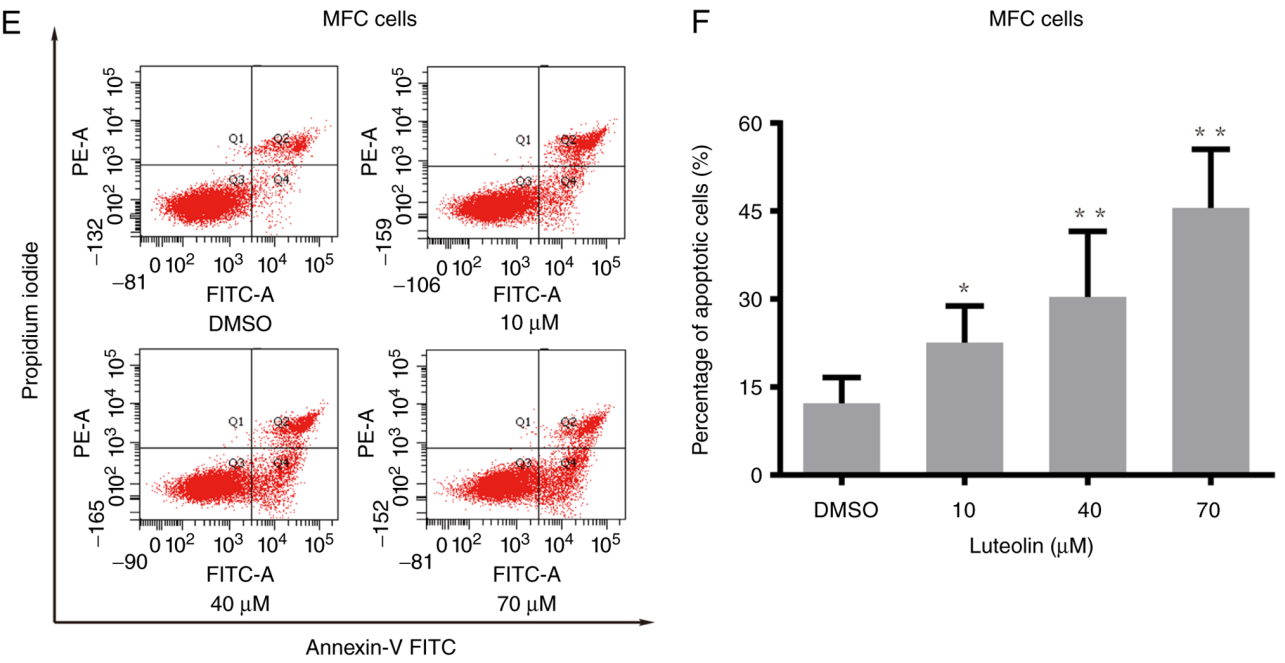

Figure 2. HGC-27 and MFC cells apoptosis are induced by luteolin. Morphological changes indicative of (A) HGC-27 cells and (B) MFC cells apoptosis were observed using Hoechst 33258 staining method under an inverted fluorescence microscope (magnification, x100). Red arrows indicated the apparent apoptotic morphological features, such as karyopyknosis, nucleosome and chromosome condensation. Following double-staining with Annexin-V FITC and PI, the flow cytometry was used to test the apoptosis in (C) HGC-27 cells and (E) MFC cells, and the quantitative determination of apoptosis of (D) HGC-27 cells and (F) MFC cells was showed on the histogram. Experiments were repeated at least three times. *P<0.05 and **P<0.01 vs. DMSO group. HGC-27, human gastric cancer HGC-27 cell line; MFC, mouse forestomach carcinoma cell line.

group. Due to the luteolin treatment, the cell morphology become irregular.

To explore whether apoptosis was involved in the reduction of cell number induced by luteolin, morphology assessment and flow cytometry were used to detect apoptosis. HGC-27 and MFC cells were treated with luteolin (10, 40, and 70 μM) for 24 h, and MKN-45 cells were treated for 48 h. Morphological features of luteolin-induced apoptosis were detected by Hoechst 33258 staining on a fluorescence inversion microscope system. As shown in Figs. 2A, B, and S2A, apparent morphological features, such as karyopyknosis, nucleosome and chromosome condensation, were observed in the luteolin groups, while fewer apoptotic characteristics were found in the DMSO group. HGC-27, MFC, and MKN-45 cells stained with Annexin-V FITC and PI were quantified by flow cytometry. The percentage of apoptotic cells increased in a concentration-dependent manner in HGC-27 cells (Fig. 2C and D), MFC cells (Fig. 2E and F), and MKN-45 cells (Fig. S2B and S2C). These results showed that apoptosis might be largely involved in the inhibition of HGC-27, MFC, and MKN-45 cells' proliferation induced by luteolin.

Luteolin influenced ROS accumulation in gastric cancer cells. Oxidative stress plays a crucial role in cancer pathophysiology (4). ROS can cause the apoptosis of cancer cells via oxidative stress (26). Luteolin, as a flavonoid, regulates the cellular redox state. DCFH-DA staining and flow cytometry were performed to illustrate luteolin-induced ROS accumulation in HGC-27, MFC and MKN-45 cells. HGC-27 and MFC cells were treated with luteolin (10, 40, and 70 μM) for 24 h, and MKN-45 cells were treated for 48 h. There was an obvious increase in green fluorescence in the luteolin groups (Figs. 3A, B, and S3A). Moreover, the peak moved to the righter with the increase of the luteolin dose in HGC-27 cells (Fig. 3C), MFC cells (Fig. 3E), and MKN-45 (Fig. S3B). The data suggested that ROS significantly increased after exposure of HGC-27 cells (Fig. 3D) and MFC cells (Fig. 3F) to luteolin. It was also observed that ROS remarkably increased in the high dose of luteolin in MKN-45 cells (Fig. S3C). In addition, an SOD activity test suggested that luteolin could induce SOD activity reduction, especially in the high dose of luteolin groups in HGC-27 and MFC cells (Fig. 3G) and in MKN-45 cells (Fig. S3D). Thus, it was inferred that ROS played a significant role in luteolin-induced apoptosis in HGC-27, MFC, and MKN-45 cells and that the increase in ROS was related to the decreased activity of antioxidative enzymes, especially SOD.

Luteolin impaired the mitochondrial potential, ATP generation and enzyme activities in gastric cancer cells. Intracellular ROS overaccumulation is one of the characteristics of mitochondrial dysfunction (27). Mitochondrial dysfunction directly leads to apoptosis (28). Here, we explored the effects of luteolin on main mitochondrial functions, such as mitochondrial membrane potential, energy metabolism, and key protein expression levels, in gastric cancer cells. Luteolin-treated HGC-27, MFC, and MKN-45 cells were stained with JC-1 and analyzed using flow cytometry. The flow cytometry results revealed that the ratio of red/green fluorescence dramatically decreased in the luteolin groups (Figs. 4A, C, and S4A), indicating that luteolin effectively decreased the mitochondrial membrane potential of HGC-27 cells (Fig. 4B), MFC cells (Fig. 4D), and MKN-45

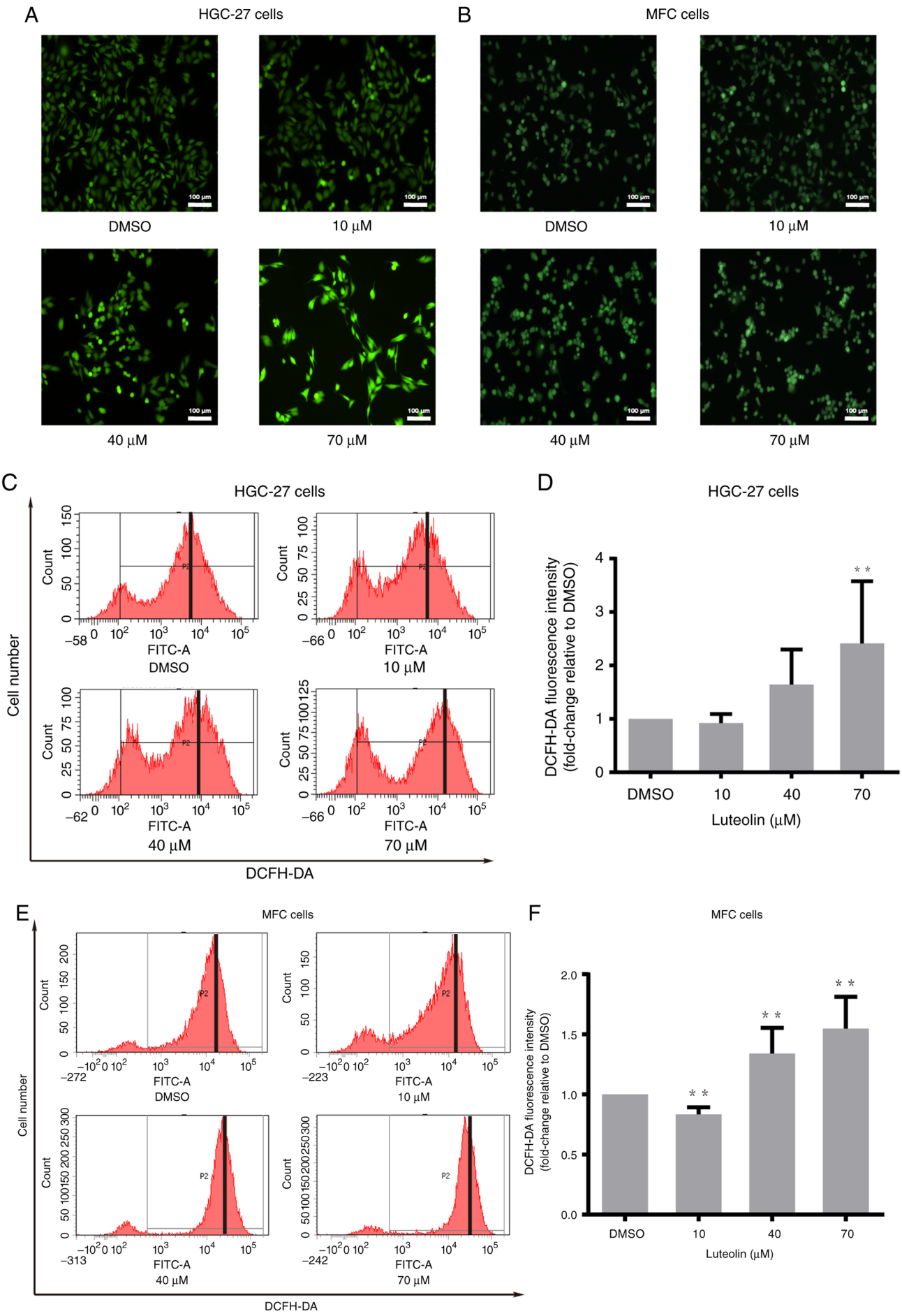

Figure 3. Continued.

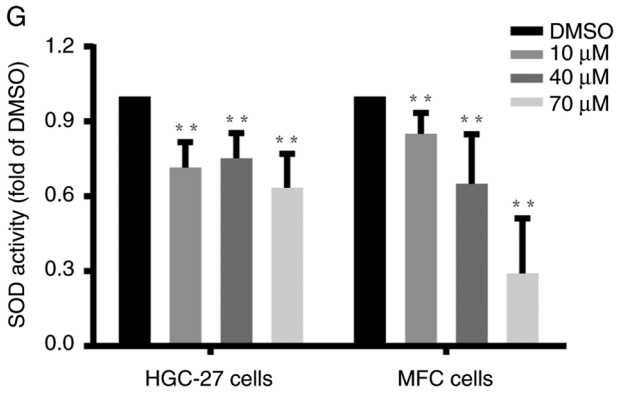

Figure 3. ROS accumulation in HGC-27 and MFC cells is induced by luteolin. The fluorescence intensity of (A) HGC-27 cells and (B) MFC cells were visualized under a fluorescence inverted microscope (magnification, x100). Luteolin-induced ROS levels were detected using DCFH-DA staining and flow cytometry in (C) HGC-27 cells and (E) MFC cells. The quantitative analysis of ROS levels in (D) HGC-27 cells and (F) MFC cells was showed on the histogram. (G) SOD activity was assessed in HGC-27 and MFC cells using a microplate reader at an absorbance of 560 nm. Experiments were repeated at least in triplicate. Data were presented as mean ± SD. **P<0.01 vs. DMSO group. ROS, reactive oxygen species; SOD, superoxide dismutase; HGC-27, human gastric cancer HGC-27 cell line; MFC, mouse forestomach carcinoma cell line.

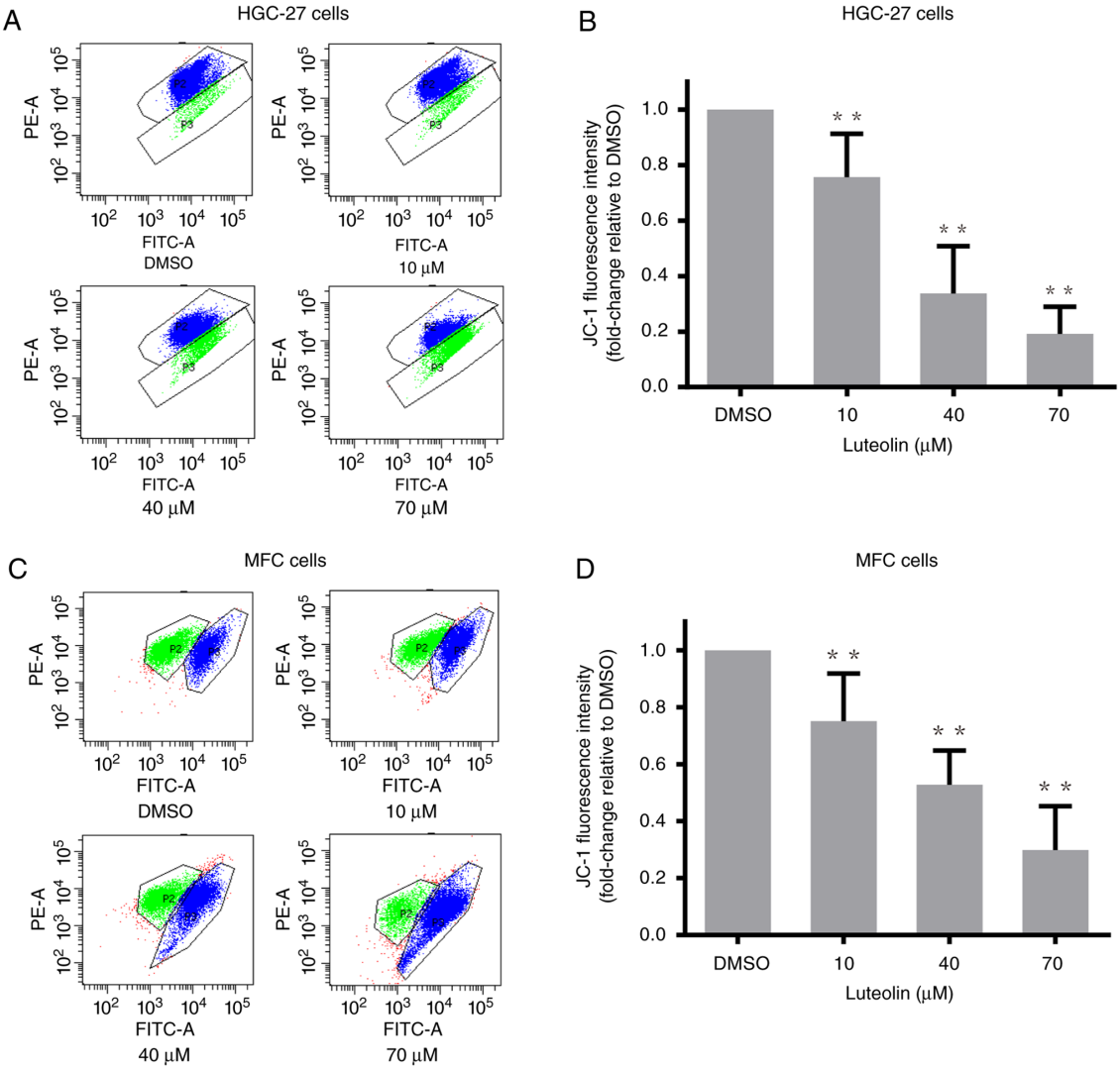

Figure 4. Continued.

cells (Fig. S4B). Next, an ATP content assay was carried out to examine the effects of luteolin on mitochondrial energy metabolism. ATP content decreased, especially in the high-dose groups (Figs. 4E and S4C). These results

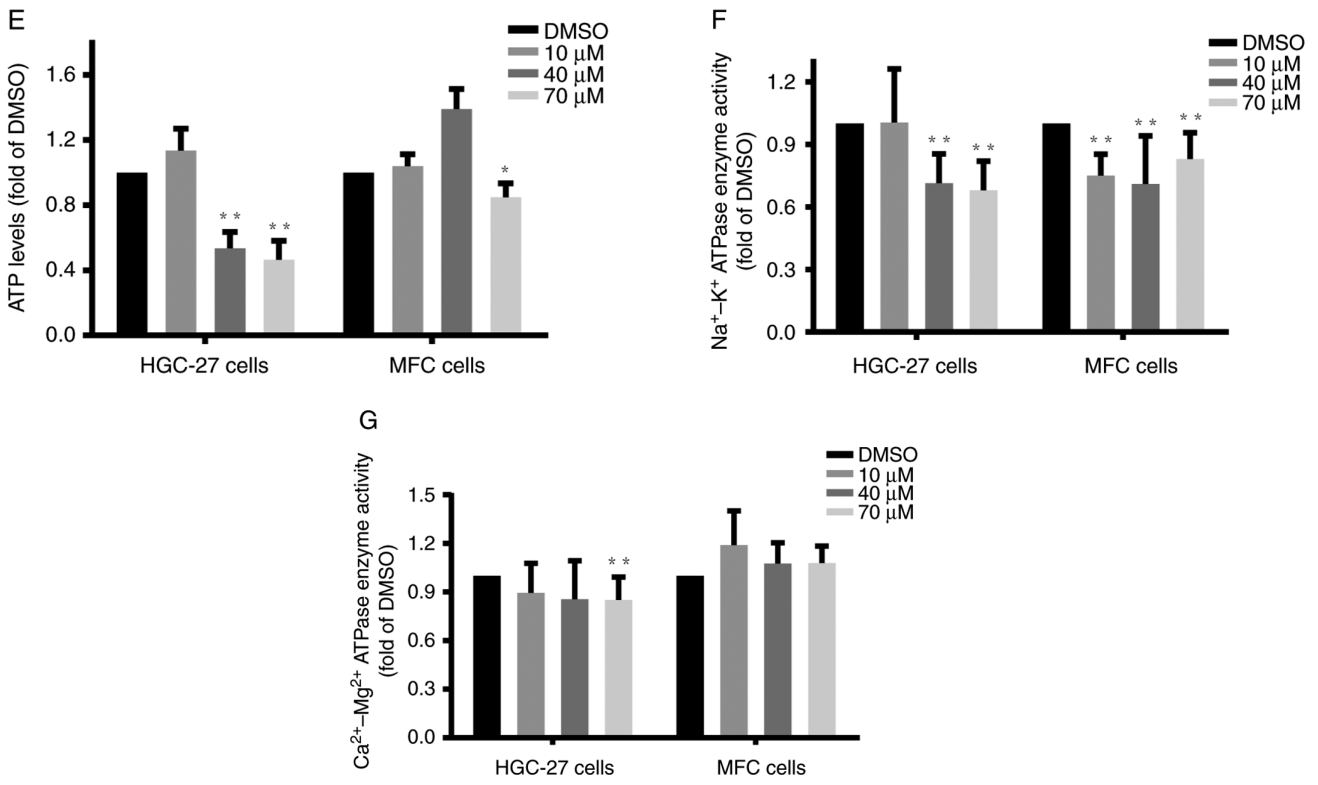

Figure 4. Mitochondrial membrane potential, ATP levels and some enzyme activities in HGC-27 and MFC cells induced by luteolin. The luteolin-treated (A) HGC-27 cells and (C) MFC cells were stained with JC-1, and analyzed using flow cytometry. Quantitative statistics of the mitochondrial membrane potential was based on flow cytometry in (B) HGC-27 cells and (D) MFC cells. The (E) ATP levels, (F) Na^+/K^+-ATPase activities and (G) Ca^{2+}/Mg^{2+}-ATPase activities were showed based on the microplate system at the absorbance values of 660 nm. The data were presented as mean ± SD. The experiments were repeated in triplicate. $^*P<0.05$, $^{**}P<0.01$ vs. DMSO group. HGC-27, human gastric cancer HGC-27 cell line; MFC, mouse forestomach carcinoma cell line.

demonstrated that luteolin could remarkably reduce ATP levels, suggesting that luteolin produced deleterious effects on mitochondrial energy generation in HGC-27, MFC, and MKN-45 cells. Following the decrease in ATP contents, luteolin effectively downregulated plasma membrane-bound Na^+/K^+-ATPase (Fig. 4F) and Ca^{2+}/Mg^{2+}-ATPase (Fig. 4G) enzyme activities, especially in the high-dose groups in HGC-27 cells, indicating that luteolin impaired the membrane permeability.

Luteolin inhibited the activities of key enzymes of the METC in gastric cancer cells. The METC complexes, located at the inner mitochondrial membrane, are coupled with respiratory electron transfer and ATP synthesis (29). Complexes I and III are closely associated with ROS generation, whereas complex V is primarily responsible for ATP production. Complexes I, III, and V play critical roles in cancer cell apoptosis (30). HGC-27, MFC, and MKN-45 cells at the logarithmic phase were treated with luteolin as mentioned previously, and specific assay kits were employed to examine the changes in the activities of complexes I (31), III, and V (25). The enzymes activities of complex I (Figs. 5A and S5A), complex III (Fig. 5B), and complex V (Figs. 5C and S5B) significantly decreased compared with the DMSO group, indicating that luteolin exerted inhibitory effects on the activities of METC complexes I, III, and V, especially in the high dose of luteolin groups in HGC-27, MFC, and MKN-45 cells. These findings suggested that luteolin could exert inhibitory effects on METC complex activities in HGC-27 and MFC cells in a dose-dependent manner. And high dose of luteolin could effectively inhibit METC complexes I and V activities in MKN-45 cells.

Luteolin unbalanced Bcl-2 and Bax protein expression in gastric cancer cells. Bcl-2 family members are involved in modulating the mitochondrial permeability transition (32) and regulating the integrity and function of the outer mitochondrial membrane (33). Bcl-2 and Bax are core regulators of the intrinsic pathway of apoptosis in response to stress stimuli (33). Further, they play important roles in regulating the permeabilization of the outer mitochondrial membrane (34). Western blot findings demonstrated that luteolin significantly decreased the ratio between Bcl-2 and Bax in HGC-27, MFC, and MKN-45 cells (Figs. 6C and S6B) by downregulating Bcl-2 expression (Figs. 6B and S6A) and/or upregulating Bax expression (Figs. 6A and S6A). Thus, these results verified that luteolin exerted destructive effects on mitochondrial function in HGC-27, MFC, and MKN-45 cells by unbalancing the expression of Bcl-2 and Bax proteins.

Discussion

Chemical compounds in natural extracts may reportedly have potential as therapeutic agents for gastric cancer (35). Luteolin is a natural ingredient found in a variety of fruits, vegetables, and herbs. The cost of luteolin has been greatly reduced, as it can now be extracted from peanut shells, which

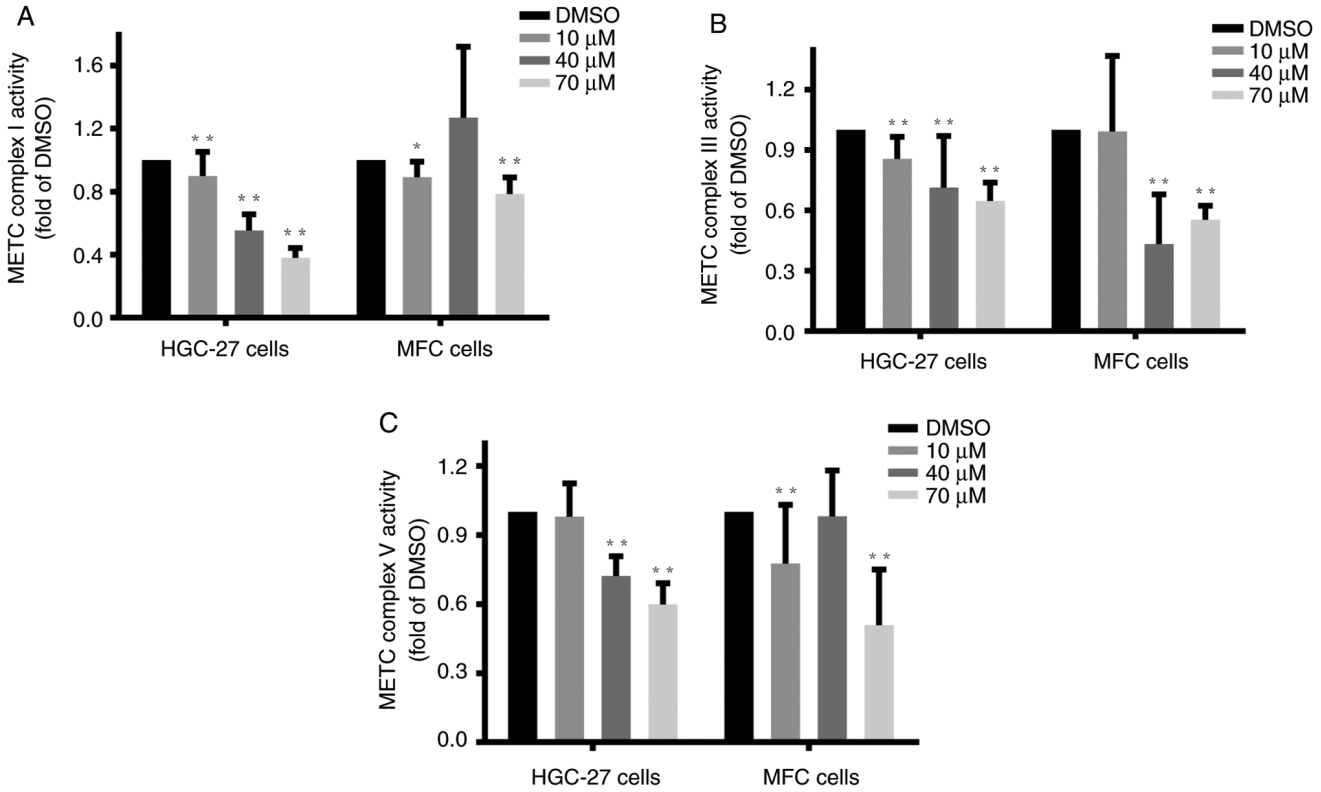

Figure 5. Luteolin induces the enzyme activities of the METC complexes in HGC-27 and MFC cells. Complexes (A) I, (B) III and (C) V were assessed by testing kits. The data were obtained using a microplate reader at 340, 550 and 660 nm, respectively. The data were presented as mean ± SD. The experiments were performed at least in triplicate. *P<0.05 and **P<0.01 vs. DMSO group; HGC-27, human gastric cancer HGC-27 cell line; MFC, mouse forestomach carcinoma cell line.

is economical for mass production and clinical practice (36). Therefore, several studies have been conducted to reveal many biological effects of luteolin, including anti-inflammatory (37), antioxidative (38), analgesic (39), and anticancer activities (4). Our study demonstrated that luteolin exerted significant inhibitory effects on the proliferation of HGC-27, MFC, and MKN-45 gastric cancer cells. Luteolin treatment-induced distinct morphological and biochemical features associated with apoptosis in HGC-27, MFC, and MKN-45 cells, such as chromatin condensation, membrane surface blebbing, and formation of apoptotic bodies. Thus, apoptosis is the main mechanism of luteolin-induced inhibition of cell proliferation. We also found that luteolin could effectively interfere with the redox state of gastric cancer cells. Namely, with an increased dose of luteolin, rising ROS levels were observed in HGC-27 and MFC cells. And high dose of luteolin could induce ROS increase in MKN-45 cells. It is indicated that the effect of luteolin on stimulating ROS increase is various in different cell lines. As the most significant signaling molecules, ROS participate in regulating many biological processes, such as redox state changes and apoptosis. Low ROS levels are necessary to maintain cellular signaling processes (40). In contrast, a sudden and substantial increase in ROS levels commits cells to apoptosis (28). Presumably, luteolin could induce gastric cancer cells apoptosis by elevating ROS levels. Luteolin's properties are probably predetermined by its chemical structure, which includes four phenolic hydroxyl groups in C5 and C7 of the benzene A ring and C3' and C4' of the benzene B ring. Luteolin's antioxidant activity has been attributed to the ortho-dihydroxy structure of its B-ring and the 2,3-double bond in conjugation with the 4-oxo function of the C ring (4,41).

The $\Delta\Psi$m collapse has been associated with apoptosis-related mitochondrial fragmentation, which is considered an irreversible point in the death signaling cascade (42). In this study, luteolin was shown to damage $\Delta\Psi$m as reflected by the decreased ratio of red/green fluorescence found in all luteolin groups of HGC-27, MFC, and MKN-45 cells. Several reports have shown that the sudden $\Delta\Psi$ decrease with a corresponding rise in ROS generation may be attributed to mitochondrial permeability transition pore (mPTP) induction (43). mPTP is a transmembrane channel formed at the contact sites between the inner and outer mitochondrial membranes (44). There is evidence that brief mPTP openings are critical to maintaining healthy mitochondrial homeostasis. However, when ROS accumulation exceeds the threshold, it leads to longer mPTP openings, resulting in an ROS burst release (43). This regenerative cycle of mitochondrial ROS formation and release was defined as ROS-induced ROS release (RIRR) (43). Longer mPTP openings possibly play a physiological role in luteolin-induced gastric cancer apoptosis. The mPTP formation leads to the mitochondrial permeability transition (MPT), which was modulated by Bcl-2 family members (32). The Bcl-2 family proteins, including antiapoptotic (Bcl-2) and proapoptotic (Bax) members, can form ion channels when incorporated into synthetic lipid bilayers (33). mPTP is regulated by proapoptoic and antiapoptotic Bcl-2 family proteins, such as Bax and Bcl-2, through the composition of the voltage-dependent anion channel (VDAC) (45). Moreover,

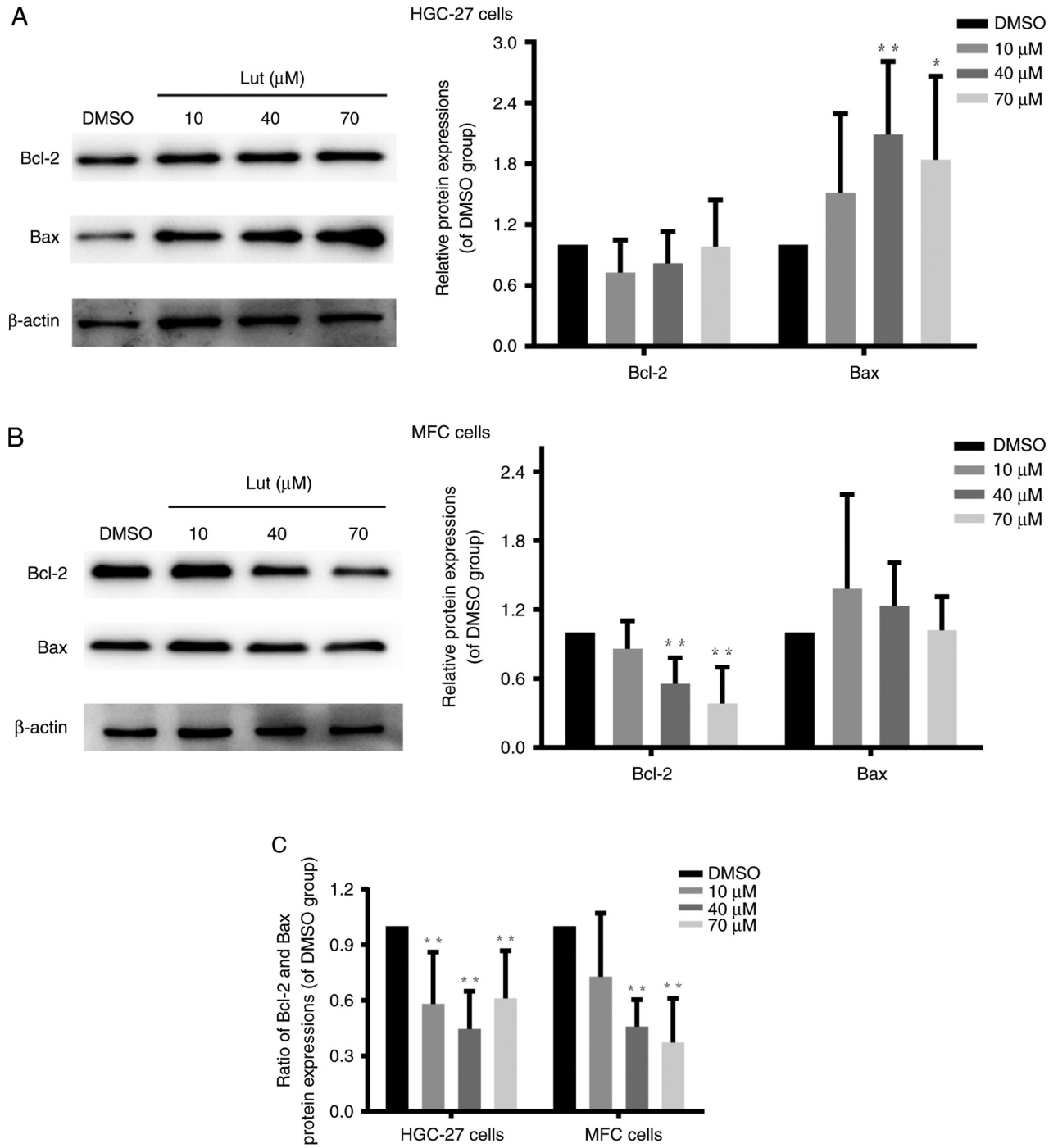

Figure 6. Luteolin unbalanced Bcl-2 and Bax protein expression in HGC-27 and MFC cells. Bcl-2 and Bax protein levels in (A) HGC-27 cells and (B) MFC cells were examined using western blot. (C) Ratio between Bcl-2 and Bax protein expression levels is showed in the histogram. The data were presented as mean ± SD. Experiments were repeated at least in triplicate. *P<0.05 and **P<0.01 vs. DMSO group. Bcl-2, B cell lymphoma-2; Bax, Bcl-2-associated X; HGC-27, human gastric cancer HGC-27 cell line; MFC, mouse forestomach carcinoma cell line.

members of the Bcl-2 family, such as Bcl-2 and Bax, are involved in regulating the integrity and function of the outer mitochondrial membrane (33). Unbalanced expressions of Bcl-2 and Bax proteins is involved in the apoptosis induced by luteolin in cancer cells (46). Our data demonstrated that luteolin remarkably decreased the ratio of Bcl-2 and Bax by downregulating Bcl-2 protein expression and/or upregulating Bax protein expression in three gastric cancer cell lines. Therefore, we inferred that luteolin might induce longer mPTP formation and destroy the outer mitochondrial membrane by unbalancing Bcl-2 and Bax protein expression in HGC-27, MFC, and MKN-45 cells, leading to apoptosis.

Luteolin induced $\Delta\Psi m$ decrease and ROS increase, resulting in disrupting the proton-motive force. Then, the integrity of the inner mitochondrial membrane is impaired, and the oxidative phosphorylation is uncoupled (47). METCs are located on the inner mitochondrial membrane, where complexes I, III, and IV are proton pumps, while CoQ and

cytochrome c are electron carriers (13). METC is the central player in the chemiosmotic theory, in which the proton circuit across the inner mitochondrial membrane actuates the oxidative phosphorylation, coupling substrate oxidation and adenosine 5'-diphosphate (ADP) phosphorylation (29). Substrate oxidation releases electrons to cofactors, such as nicotinamide adenine dinucleotide (NADH) or 1,5-dihydroflavin adenine dinucleotide (FADH2). These electrons pass through electron carriers of METC complexes with increasing oxidation potentials, ultimately reducing molecular oxygen to water (48). Electrons carried by NADH are transferred to the flavin mononucleotide (I_F) site in complex I, where they are normally passed down the chain of Fe-S centers to the ubiquinone-binding site (I_Q). At both the I_F and I_Q sites, electrons react with O_2, forming superoxide ($O_2^{\bullet-}$) within the mitochondrial matrix (13,49). In complex III, QH_2 binds to the Q_O site, and electrons are transferred in the Q-cycle and react directly with oxygen to form superoxide that is released to both sides of the inner mitochondrial membrane (50).

In our study, luteolin downregulated the activities of complexes I and III in HGC-27 and MFC cells, resulting in luteolin-induced ROS generation and mitochondrial dysfunction. And high dose of luteolin could exert more effective inhibition on complex I in MKN-45 cells. This might have occurred, because luteolin inhibited enzyme activities by binding to the quinone-binding site of the complexes, backing up electrons in the chain of Fe-S clusters and leading to rapid ROS generation (51). In addition to luteolin, plant-derived chemicals with anticancer activity directed against METC complexes include resveratrol (52), xanthohumol (14), and deguelin (53). As inhibition of METC complexes is associated with increased ROS production, targeting METC complexes to increase ROS production is a plausible and intriguing strategy to eliminate cancer cells with relatively high specificity (28). Moreover, the ATP level was reduced in the high dose of luteolin groups. In line with the ATP content, METC complex V activity was remarkably reduced by luteolin. ATP is mainly derived from the METC complex V, which can convert the proton gradient created by METC complexes I-IV into ATP by phosphorylating ADP (28). Therefore, decreased METC complex V activity induced by luteolin is the leading cause of ATP reduction, which can impair mitochondrial function. ATP downregulation also reduces ATP-dependent Na^+/K^+-ATPase and Ca^{2+}/Mg^{2+}-ATPase enzyme activities, destroying cellular membrane permeability and promoting the apoptosis. This suggests that luteolin may impair mitochondrial function and membrane ionic equilibrium by increasing ROS and decreasing ATP synthesis, where METC downregulation is indispensable.

In addition, it is reported that luteolin could induce cell cycle arrest and apoptosis through extrinsic and intrinsic signaling pathways in MCF-7 breast cancer cell (46). The cells from different tissues have different reaction to luteolin treatment. And different tissues trigger different signaling pathway induced by luteolin. We tested the ROS change, ATP content, and mitochondrial electron transport chain complexes activities, which are the indicators of mitochondrial function. Our study found that luteolin could downregulate the activities of mitochondrial electron transport chain complexes, which are distinctively important for cell survival, cell carcinogenesis, and cell energy supply. So we propose that luteolin induces the apoptosis by interfering the cellular energy metabolism of the mitochondria in gastric cancer cells.

This study was conducted *in vitro* to demonstrate the anti-gastric cancer effects of luteolin and to reveal the underlying mechanism. Luteolin unbalanced ROS levels and ATP generation by destroying the mitochondrial membrane potential and downregulating the enzyme activities of METC complexes (mainly complexes I, III, and V). Luteolin also impaired mitochondrial integrity and function by unbalancing the protein expression of Bcl-2 family members (Bcl-2 and Bax), eventually inducing apoptosis of gastric cancer cells. Therefore, the intrinsic apoptosis pathway was involved in luteolin's anti-gastric cancer effects, and mitochondria were the main target in luteolin-induced gastric cancer apoptosis.

Acknowledgements

This study was conducted in the laboratory of the Taishan Scholars Construction Engineering of Shandong Province and the Yantai High-End Talent Introduction Plan 'Double Hundred', (Yantai, China).

Funding

This study was supported by the National Natural Science Foundation of China (grant no. 31471338), the Key Research and Development Program of Shandong Province of China (grant no. 2019GSF108214) and the Natural Science Foundation of Shandong Province (grant no. ZR2016HB51).

Availablity of data and materials

The datasets used and/or analyzed during the current study are available from the corresponding author on reasonable request.

Authors' contributions

JM conceived the work and wrote the manuscript. JM carried out the experiments and analyzed the data. ZP provided the assistance on the experiments. XC and XZ performed the data analysis and provided technical support. HD and WH offered guidance and support, and assisted in the acquisition of data. QZ and XT designed the experiments and reviewed the manuscript. All authors read and approved the final manuscript. JM and QZ confirm the authenticity of all the raw data.

Ethics approval and consent to participate

Not applicable.

Patient consent for publication

Not applicable.

Competing interests

The authors declare that they have no competing interests.

References

1. Xiao S and Zhou L: Gastric cancer: Metabolic and metabolomics perspectives (Review). Int J Oncol 51: 5-17, 2017.
2. Song Z, Wu Y, Yang J, Yang D and Fang X: Progress in the treatment of advanced gastric cancer. Tumour Biol 39: 1010428317714626, 2017.
3. Falah M, Rayan M and Rayan A: A novel paclitaxel conjugate with higher efficiency and lower toxicity: A new drug candidate for cancer treatment. Int J Mol Sci 20: 4965, 2019.
4. Imran M, Rauf A, Abu-Izneid T, Nadeem M, Shariati MA, Khan IA, Imran A, Orhanh IE, Rizwan M, Atif M, *et al*: Luteolin, a flavonoid, as an anticancer agent: A review. Biomedicine Pharmacotherapy 112: 108612, 2019.
5. Tesio AY and Robledo SN: Analytical determinations of luteolin. Biofactors 47: 141-164, 2021.
6. Tuorkey MJ: Molecular targets of luteolin in cancer. Eur J Cancer Prev 25: 65-76, 2016.
7. Mani S, Swargiary G and Singh KK: Natural agents targeting mitochondria in cancer. Int J Mol Sci 21: 6992, 2020.
8. Gong G, Jiao Y, Pan Q, Tang H, An Y, Yuan A, Wang K, Huang C, Dai W, Lu W, *et al*: Antitumor effect and toxicity of an albumin-paclitaxel nanocarrier system constructed via controllable alkali-induced conformational changes. ACS Biomater Sci Eng 5: 1895-1906, 2019.
9. Xu X, Lai Y and Hua ZC: Apoptosis and apoptotic body: Disease message and therapeutic target potentials. Biosci Rep 39: BSR20180992, 2019.
10. Yang Y, He PY, Zhang Y and Li N: Natural products targeting the mitochondria in cancers. Molecules 26: 92, 2020.
11. Kalpage HA, Wan J, Morse PT, Zurek MP, Turner AA, Khobeir A, Yazdi N, Hakim L, Liu J, Vaishnav A, *et al*: Cytochrome c phosphorylation: Control of mitochondrial electron transport chain flux and apoptosis. Int J Biochem Cell Biol 121: 105704, 2020.
12. He C, Jiang S, Jin H, Chen S, Lin G, Yao H, Wang X, Mi P, Ji Z, Lin Y, *et al*: Mitochondrial electron transport chain identified as a novel molecular target of SPIO nanoparticles mediated cancer-specific cytotoxicity. Biomaterials 83: 102-114, 2016.
13. Zhao RZ, Jiang S, Zhang L and Yu ZB: Mitochondrial electron transport chain, ROS generation and uncoupling (Review). Int J Mol Med 44: 3-15, 2019.
14. Zhang B, Chu W, Wei P, Liu Y and Wei T: Xanthohumol induces generation of reactive oxygen species and triggers apoptosis through inhibition of mitochondrial electron transfer chain complex I. Free Radic Biol Med 89: 486-497, 2015.
15. Yang Q, Wang L, Liu J, Cao WL, Pan Q and Li M: Targeting the complex I and III of mitochondrial electron transport chain as a potentially viable option in liver cancer management. Cell Death Discovery 7: 293, 2021.
16. Yuan Y, Zhai Y, Chen J, Xu X and Wang H: Kaempferol ameliorates oxygen-glucose deprivation/reoxygenation-induced neuronal ferroptosis by activating Nrf2/SLC7A11/GPX4 axis. Biomolecules 11: 923, 2021.
17. Wang Y, Pan Z, Cheng XL, Zhang K, Zhang X, Qin Y, Fan J, Yan T, Han T, Shiu KK, *et al*: A red-light-activated sulfonamide porphycene for highly efficient photodynamic therapy against hypoxic tumor. Eur J Med Chem 209: 112867, 2021.
18. Hu T, Linghu K, Huang S, Battino M, Georgiev MI, Zengin G, Li D, Deng Y, Wang YT and Cao H: Flaxseed extract induces apoptosis in human breast cancer MCF-7 cells. Food Chem Toxicol 127: 188-196, 2019.
19. Zhang X, Qin Y, Pan Z, Li M, Liu X, Chen X, Qu G, Zhou L, Xu M, Zheng Q and Li D: Cannabidiol induces cell cycle arrest and cell apoptosis in human gastric cancer SGC-7901 cells. Biomolecules 9: 302, 2019.
20. Lei L, Zhu Y, Gao W, Du X, Zhang M, Peng Z, Fu S, Li X, Zhe W, Li X and Liu G: Alpha-lipoic acid attenuates endoplasmic reticulum stress-induced insulin resistance by improving mitochondrial function in HepG2 cells. Cell Signal 28: 1441-1450, 2016.
21. Pan Z, Luo Y, Xia Y, Zhang X, Qin Y, Liu W, Li M, Liu X, Zheng Q and Li D: Cinobufagin induces cell cycle arrest at the S phase and promotes apoptosis in nasopharyngeal carcinoma cells. Biomed Pharmacother 122: 109763, 2020.
22. Dergousova EA, Petrushanko IY, Klimanova EA, Mitkevich VA, Ziganshin RH, Lopina OD and Makarov AA: Enhancement of Na,K-ATPase activity as a result of removal of redox modifications from cysteine residues of the a1 subunit: The effect of reducing agents. Mol Biol (Mosk) 52: 247-250, 2018 (In Russian).
23. Lin J, Zhao HS, Xiang LR, Xia J, Wang LL, Li XN, Li JL and Zhang Y: Lycopene protects against atrazine-induced hepatic ionic homeostasis disturbance by modulating ion-transporting ATPases. J Nutr Biochem 27: 249-256, 2016.
24. Yang Y, Li J, Wei C, He Y, Cao Y, Zhang Y, Sun W, Qiao B and He J: Amelioration of nonalcoholic fatty liver disease by swertiamarin in fructose-fed mice. Phytomedicine 59: 152782, 2019.
25. OuYang Q, Tao N and Zhang M: A damaged oxidative phosphorylation mechanism is involved in the antifungal activity of citral against *Penicillium digitatum*. Front Microbiol 9: 239, 2018.
26. Hanikoglu A, Ozben H, Hanikoglu F and Ozben T: Hybrid compounds & oxidative stress induced apoptosis in cancer therapy. Curr Med Chem 27: 2118-2132, 2020.
27. Yang Y, Karakhanova S, Hartwig W, D'Haese JG, Philippov PP, Werner J and Bazhin AV: Mitochondria and mitochondrial ROS in cancer: Novel targets for anticancer therapy. J Cell Physiol 231: 2570-2581, 2016.
28. Zhu Y, Dean AE, Horikoshi N, Heer C, Spitz DR and Gius D: Emerging evidence for targeting mitochondrial metabolic dysfunction in cancer therapy. J Clin Invest 128: 3682-3691, 2018.
29. Guo R, Gu J, Zong S, Wu M and Yang M: Structure and mechanism of mitochondrial electron transport chain. Biomed J 41: 9-20, 2018.
30. Luo Y, Ma J and Lu W: The significance of mitochondrial dysfunction in cancer. Int J Mol Sci 21: 5598, 2020.
31. Zhu H, Zhang W, Zhao Y, Shu X, Wang W, Wang D, Yang Y, He Z, Wang X and Ying Y: GSK3β-mediated tau hyperphosphorylation triggers diabetic retinal neurodegeneration by disrupting synaptic and mitochondrial functions. Mol Neurodegener 13: 62, 2018.
32. Means RE and Katz SG: Balancing life and death: BCL-2 family members at diverse ER-mitochondrial contact sites. FEBS J 289: 7075-7112, 2022.
33. Edlich F: BCL-2 proteins and apoptosis: Recent insights and unknowns. Biochem Biophys Res Commun 500: 26-34, 2018.
34. Peña-Blanco A and García-Sáez AJ: Bax, bak and beyond-mitochondrial performance in apoptosis. FEBS J 285: 416-431, 2018.
35. Lee YK, Bae K, Yoo HS and Cho SH: Benefit of adjuvant traditional herbal medicine with chemotherapy for resectable gastric cancer. Integr Cancer Ther 17: 619-627, 2018.
36. Sheng S, Zhang L and Chen G: Determination of 5,7-dihydroxychromone and luteolin in peanut hulls by capillary electrophoresis with a multiwall carbon nanotube/poly(ethylene terephthalate) composite electrode. Food Chem 145: 555-561, 2014.
37. Huang XF, Zhang JL, Huang DP, Huang AS, Huang HT, Liu Q, Liu XH and Liao HL: A network pharmacology strategy to investigate the anti-inflammatory mechanism of luteolin combined with in vitro transcriptomics and proteomics. Int Immunopharmacol 86: 106727, 2020.
38. Gendrisch F, Esser PR, Schempp CM and Wölfle U: Luteolin as a modulator of skin aging and inflammation. BioFactors 47: 170-180, 2021.
39. Hashemzaei M, Abdollahzadeh M, Iranshahi M, Golmakani E, Rezaee R and Tabrizian K: Effects of luteolin and luteolin-morphine co-administration on acute and chronic pain and sciatic nerve ligated-induced neuropathy in mice. J Complement Integr Med 14: 2017.
40. Fruehauf JP and Meyskens FL Jr.: Reactive oxygen species: A breath of life or death? Clin Cancer Res 13: 789-794, 2007.
41. Zheng YZ, Chen DF, Deng G, Guo R and Fu ZM: The surrounding environments on the structure and antioxidative activity of luteolin. J Mol Model 24: 149, 2018.
42. Lu J, Wu L, Wang X, Zhu J, Du J and Shen B: Detection of mitochondria membrane potential to study CLIC4 knockdown-induced HN4 cell apoptosis in vitro. J Vis Exp: 56317, 2018.
43. Zorov DB, Juhaszova M and Sollott SJ: Mitochondrial reactive oxygen species (ROS) and ROS-induced ROS release. Physiol Rev 94: 909-950, 2014.
44. Bauer TM and Murphy E: Role of mitochondrial calcium and the permeability transition pore in regulating cell death. Circ Res 126: 280-293, 2020.
45. Dudko HV, Urban VA, Davidovskii AI and Veresov VG: Structure-based modeling of turnover of Bcl-2 family proteins bound to voltage-dependent anion channel 2 (VDAC2): Implications for the mechanisms of proapoptotic activation of bak and bax in vivo. Comput Biol Chem 85: 107203, 2020.

46. Park SH, Ham S, Kwon TH, Kim MS, Lee DH, Kang JW, Oh SR and Yoon DY: Luteolin induces cell cycle arrest and apoptosis through extrinsic and intrinsic signaling pathways in MCF-7 breast cancer cells. J Environ Pathol Toxicol Oncol 33: 219-231, 2014.
47. Beutner G, Alavian KN, Jonas EA and Porter GA Jr: The mitochondrial permeability transition pore and ATP synthase. Handb Exp Pharmacol 240: 21-46, 2017.
48. Fernandez-Vizarra E and Zeviani M: Mitochondrial disorders of the OXPHOS system. FEBS Lett 595: 1062-1106, 2021.
49. Cogliati S, Lorenzi I, Rigoni G, Caicci F and Soriano ME: Regulation of mitochondrial electron transport chain assembly. J Mol Biol 430: 4849-4873, 2018.
50. Affourtit C, Wong HS and Brand MD: Measurement of proton leak in isolated mitochondria. Methods Mol Biol 1782: 157-170, 2018.
51. Larosa V and Remacle C: Insights into the respiratory chain and oxidative stress. Bioscience Reports 38: BSR20171492, 2018.
52. de Oliveira MR, Nabavi SF, Manayi A, Daglia M, Hajheydari Z and Nabavi SM: Resveratrol and the mitochondria: From triggering the intrinsic apoptotic pathway to inducing mitochondrial biogenesis, a mechanistic view. Biochim Biophys Acta 1860: 727-745, 2016.
53. Preston S, Korhonen PK, Mouchiroud L, Cornaglia M, McGee SL, Young ND, Davis RA, Crawford S, Nowell C, Ansell BRE, *et al*: Deguelin exerts potent nematocidal activity via the mitochondrial respiratory chain. FASEB J 31: 4515-4532, 2017.